

Azimuthal asymmetry of the coherent backscattering cone: Theoretical resultsMichael I. Mishchenko,^{1,*} Janna M. Dlugach,² and Li Liu¹¹*NASA Goddard Institute for Space Studies, 2880 Broadway, New York, New York 10025, USA*²*Main Astronomical Observatory, National Academy of Sciences of Ukraine, 27 Zabolotny Str., 03680 Kyiv, Ukraine*

(Received 29 September 2009; published 23 November 2009)

The azimuthal asymmetry of the polarized backscattering cone and the intimately related polarization opposition effect (POE) are corollaries of the theory of coherent backscattering (CB) valid in the asymptotic limit of very small particle packing density. In this paper we use numerically exact solutions of the Maxwell equations to study the evolution of these and other manifestations of CB as the packing density in a multiparticle group increases from zero to values typical of actual particle suspensions and particulate surfaces. Our results reveal a remarkable robustness of virtually all effects predicted by the low-density concept of CB and allow us to conclude that the azimuthal asymmetry and POE observed in the laboratory for densely packed discrete random media are indeed caused by CB.

DOI: [10.1103/PhysRevA.80.053824](https://doi.org/10.1103/PhysRevA.80.053824)

PACS number(s): 42.25.Bs, 42.25.Dd, 42.25.Fx, 42.25.Hz

I. INTRODUCTION

The azimuthal asymmetry of the polarized backscattering cone is a direct corollary [1,2] of the microphysical theory of coherent backscattering (CB) valid in the asymptotic limit of infinitesimally small packing density of Rayleigh scatterers [3,4]. In other words, it is assumed that the scattering particles are located in the far-field zones of each other, thereby letting the electromagnetic field scattered by one particle and exciting another particle to develop into an outgoing spherical wavelet [2,5–7]. This allows one to assign a phase to the wavelet propagating from one particle to another and ultimately to talk about constructive or destructive interference of pairs of multiply-scattered wavelets arriving at a remote observation point. However, the azimuthal asymmetry of the CB cone has allegedly been observed in controlled laboratory experiments for aqueous suspensions of small latex particles with a substantial volume packing density of 9.6% [8,9]. Furthermore, the inherently related polarization opposition effect (POE) in the form of a very narrow negative-polarization minimum at near-backscattering angles caused by unpolarized incident light [1,10] appears to have been observed for densely packed particulate surfaces [11–13]. This obviously raises the question of whether the low-packing-density concept of CB can still be valid in the case of densely packed particles.

In several recent papers [14–16] we have used numerically exact solutions of the Maxwell equations to demonstrate that many manifestations of CB do prevail in the case of packing densities exceeding 20%. However, direct computer modeling of the azimuthal asymmetry has proven to be more involved and has not been reported before. The main objective of this paper is to fill this gap. In fact, we will use direct solutions of the Maxwell equations to reproduce all previously anticipated observable manifestations of CB for discrete random media and trace their evolution as the volume density increases from essentially zero to more than 45%.

II. BASIC CONCEPTS

The natural way to introduce the mathematical concept of multiple electromagnetic scattering in a many-particle group is to derive the exact Foldy-Lax equations (FLEs) from the macroscopic Maxwell equations [2,17,18] and then convert the FLEs into an infinite order-of-scattering expansion [2,15,19]. In the framework of this formalism, each particle is uniquely and completely characterized by the respective dyadic transition operator. In many cases of practical interest the original FLEs are intractable and have to be simplified. One of such simplifications is the far-field version of the FLEs wherein it is assumed that each particle is located in the far-field zones of all the other particles forming the group [2,20]. Three fundamental ingredients of the far-field FLEs are as follows:

- (i) Each particle is now characterized by the scattering dyadic rather than by the dyadic transition operator;
- (ii) The partial field scattered by any particle i and exciting any particle j evolves into an outgoing spherical wavelet by the time it reaches particle j ; and
- (iii) Instead of the original system of volume integral equations one deals with a system of algebraic equations.

Each partial spherical wavelet is a transverse electromagnetic field and as such is characterized by a phase. This means that one can consider a multiple-scattering wave trajectory and evaluate its phase accumulated by the time it reaches the observation point. Furthermore, one can evaluate the result of the interference of two multiply-scattered waves at the observation point depending on the phase difference between the waves. This ultimately leads to the introduction of the ladder and cyclical diagrams [21,22] and to the derivation of the microphysical vector theories of radiative transfer (RT) and CB [2,15,20].

The vector RT theory is essentially the result of summing up self-interference results, wherein a multiply-scattered wave interferes constructively with itself. The physical origin of CB is illustrated schematically in Fig. 1(a) which shows a layer of discrete random medium illuminated by a plane-wave incident in the direction of the unit vector $\hat{\mathbf{n}}^{\text{inc}}$ and observed from a distant observation point. Consider the in-

*Author to whom correspondence should be addressed; mmishchenko@giss.nasa.gov

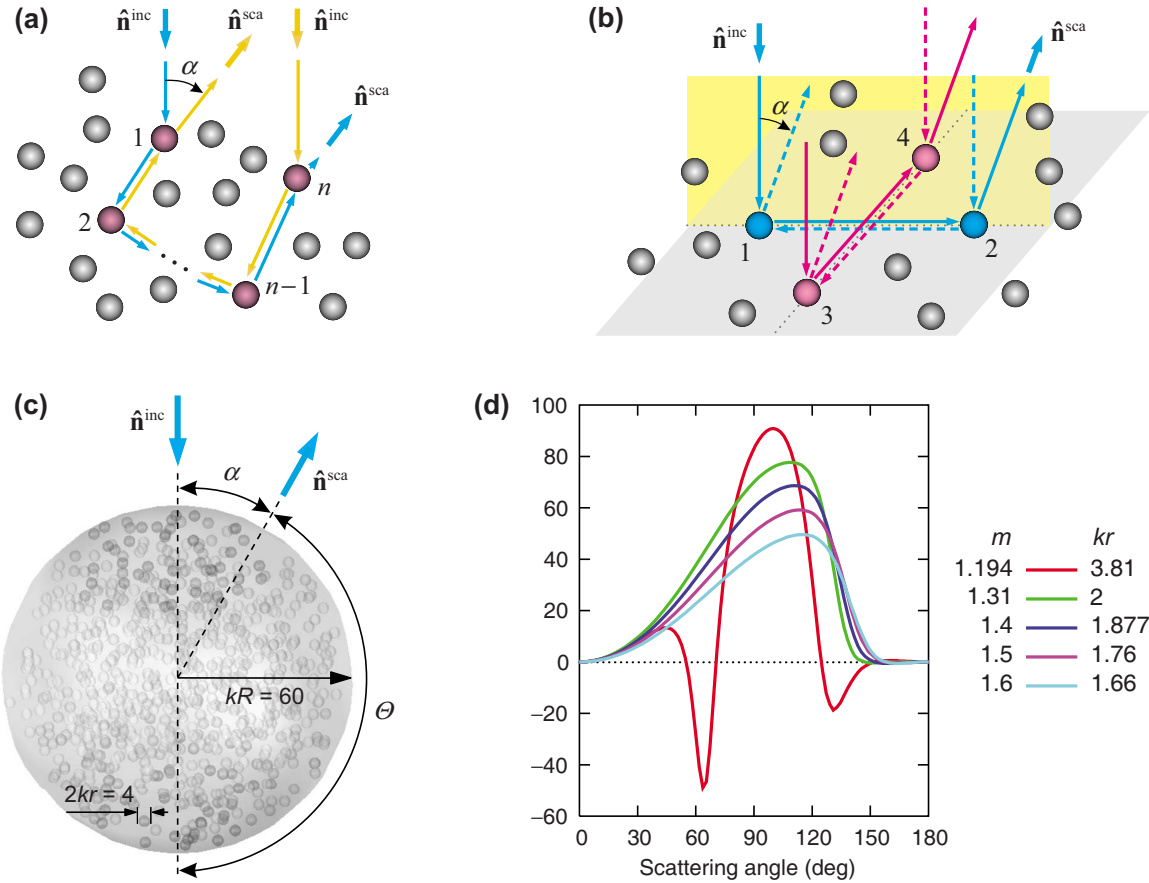


FIG. 1. (Color online) (a) Interference origin of CB. The two wave paths go through the same chain of n particles, but in opposite directions. (b) Origin of the azimuthal asymmetry of the CB cone. Particles 1–4 lie in the horizontal plane normal to the scattering (vertical) plane. (c) Scattering by a $kR=60$ spherical volume randomly filled with 800 small spheres having a size parameter of $kr=2$. (d) Polarization of scattered light for unpolarized incident light (in percent) vs scattering angle for a homogeneous spherical particle with several {refractive index, size parameter} combinations.

interference of a pair of conjugate scattered waves going through the same chain of n particles but in opposite directions. If the observation (scattering) direction given by a unit vector \hat{n}^{sca} is far from the exact backscattering direction given by $-\hat{n}^{inc}$ then the effect of the interference averaged over varying particle positions is zero. Consequently, if the scattered signal is averaged over a substantial time interval then the detector responds only to the incoherent (diffuse) intensity described by the RT equation. However, if the phase angle α (i.e., the angle between the vectors \hat{n}^{sca} and $-\hat{n}^{inc}$) is zero then the phase difference between the conjugate paths involving any chain of particles vanishes. This means that the interference is always constructive, thereby resulting in the effect of CB [23–28]. It is clear that the above interference explanation of CB explicitly relies on assigning a phase to the field scattered by one particle [e.g., particle 1 in Fig. 1(a)] and exciting another particle (particle 2), which is possible in the framework of the far-field FLEs.

The most frequently studied manifestation of CB is a narrow cone of intensity centered at the exact backscattering direction. If the incident wave is linearly polarized then the cone can become azimuthally asymmetric, provided that the particles forming the medium are Rayleigh scatterers [2,9,29,30]. In other words, the angular width of the back-

scattering cone depends on the angle between the scattering plane (i.e., the plane through the vectors \hat{n}^{inc} and \hat{n}^{sca}) and the polarization direction of the incident wave. The origin of this effect is explained in Fig. 1(b). Particles 1–4 lie in a plane normal to the illumination direction. Particles 1 and 2 lie in the scattering plane, while the line through particles 3 and 4 is perpendicular to this plane. The normalized single-particle Rayleigh-scattering matrix in the standard (I , Q , U , and V) representation of polarization [2,31] is given by

$$\tilde{\mathbf{F}}_R(\Theta) = \begin{bmatrix} \frac{3}{4}(1 + \cos^2 \Theta) & -\frac{3}{4}\sin^2 \Theta & 0 & 0 \\ -\frac{3}{4}\sin^2 \Theta & \frac{3}{4}(1 + \cos^2 \Theta) & 0 & 0 \\ 0 & 0 & \frac{3}{2}\cos \Theta & 0 \\ 0 & 0 & 0 & \frac{3}{2}\cos \Theta \end{bmatrix}, \tag{1}$$

where Θ is the scattering angle (i.e., the angle between the unit vectors \hat{n}^{inc} and \hat{n}^{sca}). Let us first assume that the incident wave is polarized linearly such that the electric field vector vibrates in the scattering plane. This means that the incidence Stokes column vector is given by

$$\mathbf{I}^{\text{inc}} = \begin{bmatrix} I^{\text{inc}} \\ Q^{\text{inc}} = I^{\text{inc}} \\ 0 \\ 0 \end{bmatrix}, \quad (2)$$

provided that the scattering plane serves as the reference for defining the Stokes parameters. Equations (1) and (2) imply that in the close vicinity of the backscattering direction, the two double-scattering trajectories going through particles 1 and 2 do not contribute to the outgoing diffuse intensity since for the first scattering event $\Theta=90^\circ$. To compute the contribution of the two double-scattering trajectories going through particles 3 and 4, one needs first to rotate the reference plane by 90° around the incidence direction, thereby left-multiplying the Stokes column vector \mathbf{I}^{inc} by the rotation matrix

$$\mathbf{L}(\eta) = \begin{bmatrix} 1 & 0 & 0 & 0 \\ 0 & \cos 2\eta & -\sin 2\eta & 0 \\ 0 & \sin 2\eta & \cos 2\eta & 0 \\ 0 & 0 & 0 & 1 \end{bmatrix} \quad (3)$$

with $\eta=90^\circ$. The cumulative result is nonzero and proportional to $2 \times (6/4)^2$. The constructive interference of the corresponding waves in the case of the exact backscattering direction doubles this result.

Let us now assume that the polarization of the incident wave is such that the electric field vector vibrates perpendicularly to the scattering plane,

$$\mathbf{I}^{\text{inc}} = \begin{bmatrix} I^{\text{inc}} \\ Q^{\text{inc}} = -I^{\text{inc}} \\ 0 \\ 0 \end{bmatrix}. \quad (4)$$

Now the contribution of the two trajectories going through particles 3 and 4 vanishes, whereas the two trajectories going through particles 1 and 2 cause a nonzero contribution to the outgoing diffuse intensity proportional to $2 \times (6/4)^2$. Again, the constructive interference of the corresponding waves doubles the backscattered intensity.

A fundamental distinction between these two scenarios is that the phase difference between the two conjugate trajectories going through particles 3 and 4 is always zero, while that between the conjugate trajectories going through particles 1 and 2 is zero at $\alpha=0^\circ$ but then oscillates rapidly with increasing α . Therefore, on average, CB will enhance the contribution of the former trajectories over a wider range of phase angles than that of the latter trajectories. As a consequence, the angular width of the CB cone will be larger in the scattering plane parallel to the direction of the incident polarization than in the scattering plane normal to this direction. This effect was called in [8,9] ‘‘spatial (or azimuthal) anisotropy of the polarized cone of enhanced backscattering.’’

A closely related phenomenon is the POE observable with unpolarized incident light. Indeed, an unpolarized beam of light can be represented as an incoherent superposition of

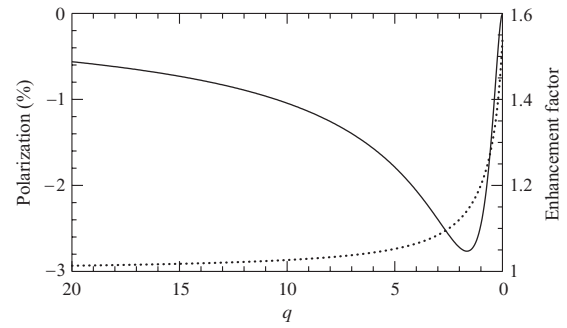


FIG. 2. Angular profiles of the enhancement factor (dotted curve) and the degree of linear polarization (solid curve) for a semi-infinite homogeneous medium composed of sparsely distributed nonabsorbing Rayleigh scatterers and illuminated by normally incident unpolarized light (after [10]). The horizontal axis shows the dimensionless angular parameter $q=kl\alpha$, where k is the wave number, α is the phase angle, and l is the transport mean-free path. The enhancement factor is defined as the ratio of the total scattered intensity to that of the diffuse background.

two linearly polarized beams with mutually perpendicular polarization directions. The above explanation of the azimuthal anisotropy then implies that in the vicinity of the backscattering direction, CB can be expected to favor scattered light polarized in the scattering plane [6,32]. The result [1,10] is a narrow negative minimum in the degree of linear polarization of the scattered light defined as

$$P = -\frac{Q^{\text{sca}}}{I^{\text{sca}}}. \quad (5)$$

The angular profile of this feature is shown in Fig. 2 along with that of the CB intensity peak. One can see that the polarization minimum is highly asymmetric and occurs at a phase angle comparable to the angular width of the coherent intensity peak.

As we have already emphasized, the very concept of CB is inherently based on the notion of wave phase and relies on the asymptotic far-field assumption. However, the conditions of far-field electromagnetic scattering are rather strict [2], require the particulate medium to have a very low-packing density, and are obviously violated in the case of densely packed scattering media wherein particles can be closely spaced and even in direct contact with each other. Yet many laboratory measurements for densely packed particle suspensions and particulate surfaces appear to show unique features predicted by the low-density theory of CB. This applies, in particular, to the observation of the spatial anisotropy of the polarized intensity cone in [8,9] as well as to the observation of the POE in [11–13]. It is, therefore, important to perform numerically exact computations of electromagnetic scattering directly based on the Maxwell equations in order to evaluate the range of applicability of the low-packing-density concept of CB. Indeed, in this case the theory can be used as an idealized ‘‘controlled laboratory experiment’’ in which all microphysical properties of the random particulate medium are known precisely and can be varied one at a time. As a consequence, the optical effects of increasing packing

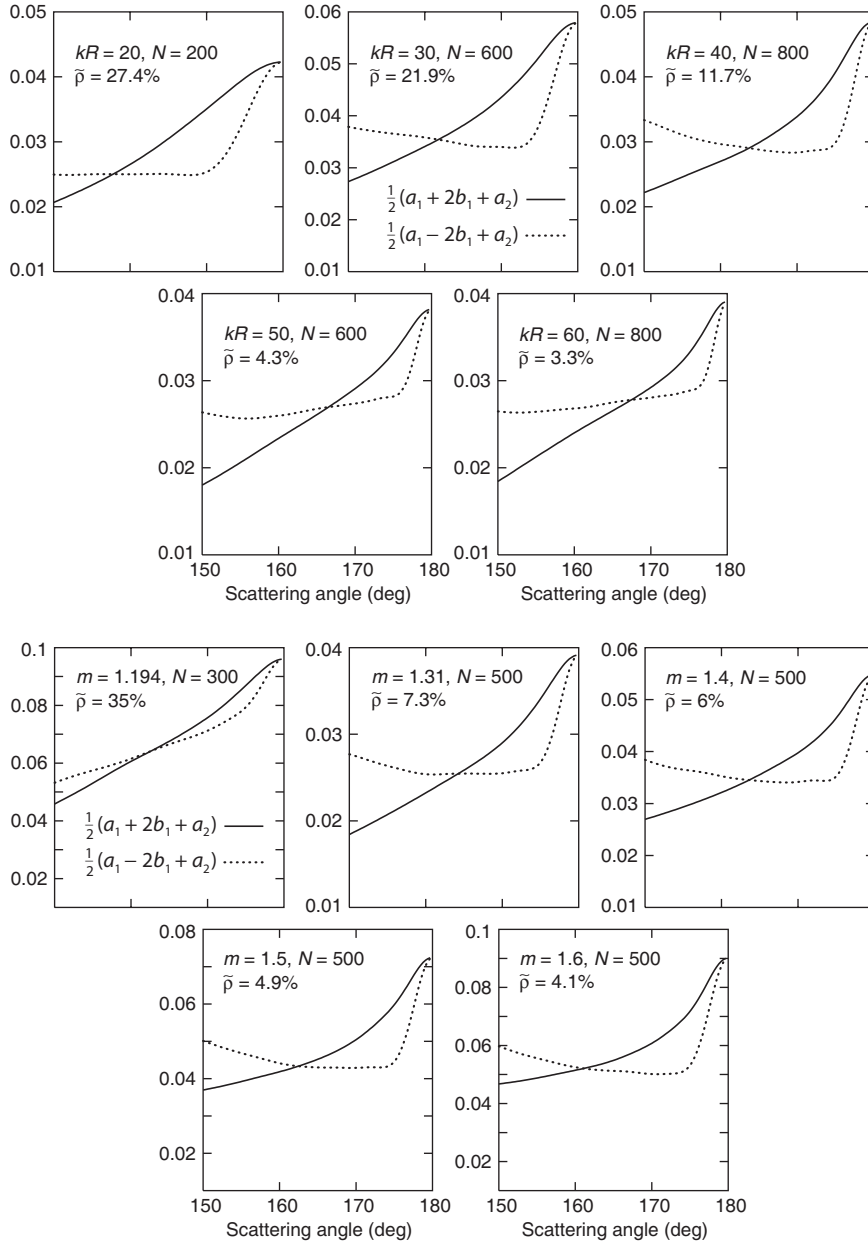


FIG. 3. Co-polarized scattered intensities defined by Eqs. (8) and (11) for a macroscopic spherical volume randomly filled with N identical particles. The particle refractive index in the five upper diagrams is fixed at $m=1.31$, while the volume size parameter kR varies from 20 to 60. The particle refractive index m in the five lower diagrams varies from 1.194 to 1.6, while the volume size parameter is fixed at $kR=40$.

density can be clearly isolated and quantified.

III. METHODOLOGY

Our model of discrete random medium is a spherical volume randomly filled with N identical nonoverlapping spherical particles as shown in Fig. 1(c). The dimension of the volume is specified in terms of its size parameter kR , where k is the wave number in the empty space surrounding the particles and R is the volume radius. The size of the particles is specified in terms of their size parameter kr , where r is the particle radius. We vary the volume size parameter from 20 to 60 and the number of particles from 1 to 900. The particle

refractive indices used in our computations are $m=1.194$ (representing latex in water), 1.31 (representing ice at visible wavelengths), 1.4, 1.5, and 1.6 (representing different mineral substances).

To model statistical randomness of particle positions within the spherical volume, we follow the approach adopted in our previous publications [14–16]. Specifically, we use one N -particle group configured randomly according to the procedure described in [33] and then average all optical observables over the uniform orientation distribution of this configuration with respect to the laboratory reference frame. This approach yields, in effect, an infinite continuous set of random realizations of the scattering volume and allows us to

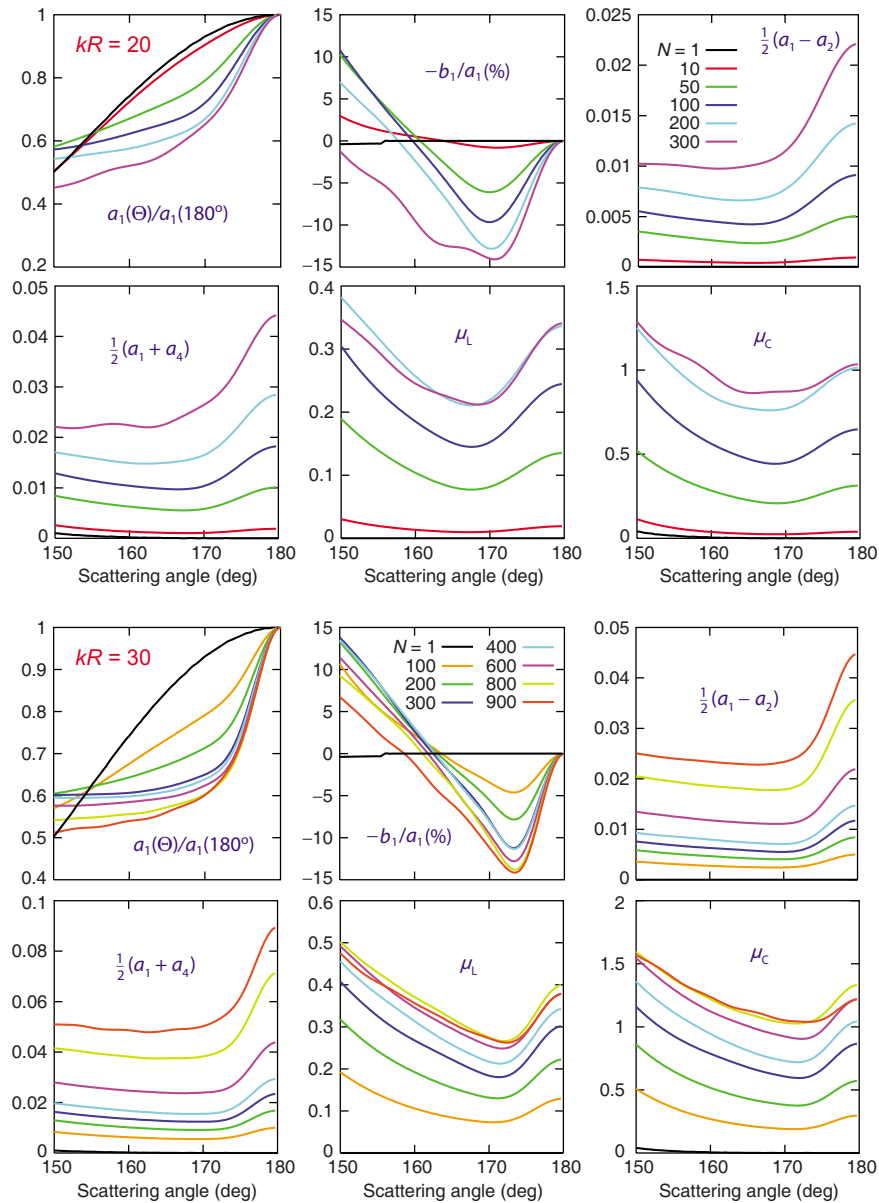


FIG. 4. (Color online) Optical characteristics of a $kR=20$ (six upper diagrams) and 30 (six lower diagrams) scattering volume randomly filled with a varying number N of $kr=2$ spherical particles. The particle refractive index is fixed at $m=1.31$. The packing density $\bar{\rho}$ varies between 1.14% ($N=10$) and 41.2% ($N=300$) for $kR=20$ and between 3.6% ($N=100$) and 32.8% ($N=900$) for $kR=30$.

use the highly efficient orientation averaging technique afforded by the superposition T -matrix method [34]. The latter represents a direct computer solver of the macroscopic Maxwell equations for a multisphere group [35,36]. Within the range of numerical convergence, the corresponding T -matrix computer program generates results with a guaranteed number of accurate decimals, which makes it numerically exact.

The relative simplicity of our model is somewhat of a concession to the current practical (but not inherent) limitations of all computer solvers of the Maxwell equations, including the superposition T -matrix method. As constructed, our model cannot be expected to replicate exactly the diverse morphologies of particulate media encountered in laboratory and natural settings. However, it appears to be sufficiently representative to permit a robust and instructive analysis of

the effects of packing density on multiple electromagnetic scattering by discrete random media.

It is assumed that the statistically random particulate volume is illuminated by a plane electromagnetic wave or a parallel quasimonochromatic beam of light propagating in the direction of the unit vector $\hat{\mathbf{n}}^{\text{inc}}$ [Fig. 1(c)]. The observation point is located in the far-field zone of the entire volume in the direction of the unit vector $\hat{\mathbf{n}}^{\text{sc}}$. Since the scattering properties of the particulate volume are averaged over all orientations of an N -particle group, they depend only on the scattering angle Θ (or on the phase angle $\alpha = \pi - \Theta$) provided that the scattering plane is used for defining the Stokes parameters of the incident and scattered light. The far-field transformation of the Stokes parameters upon the scattering by the entire volume is then written in terms of the normal-

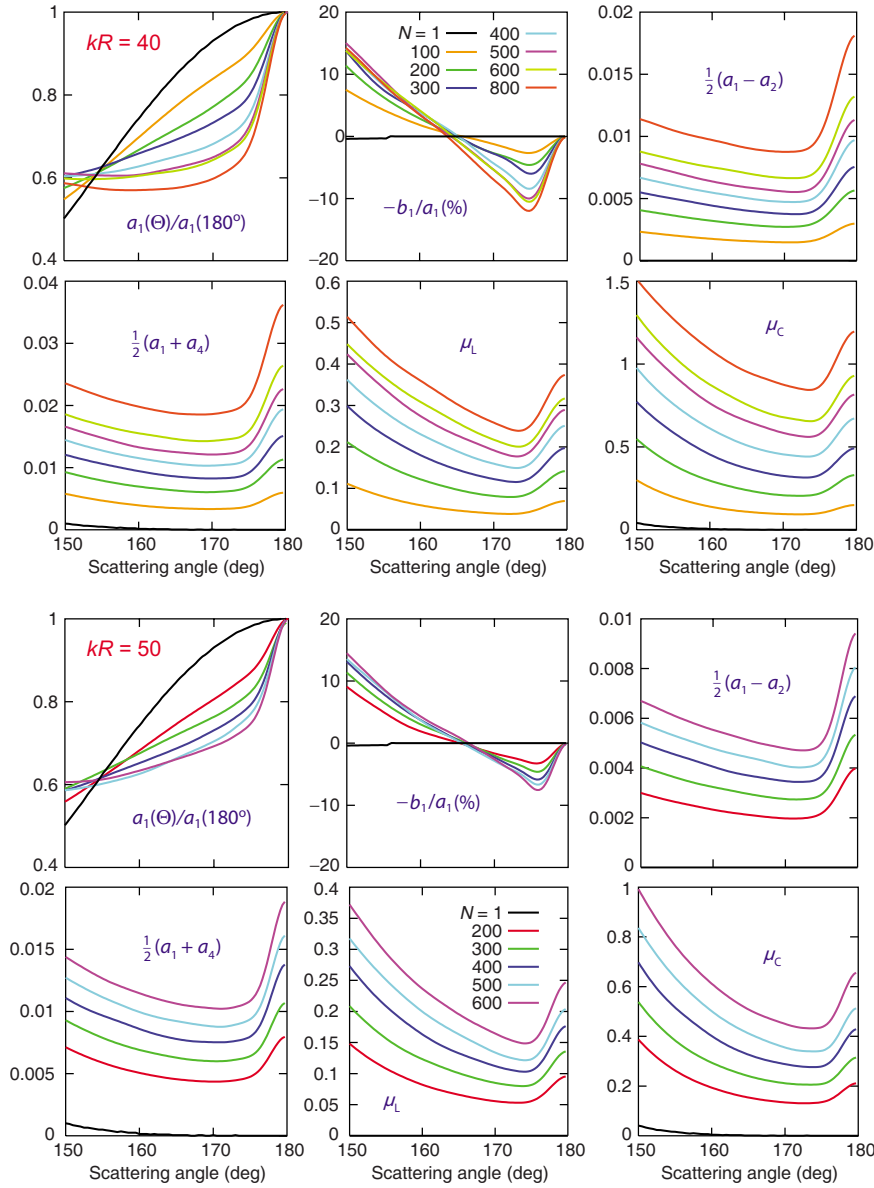


FIG. 5. (Color online) Optical characteristics of a $kR=40$ (six upper diagrams) and 50 (six lower diagrams) scattering volume randomly filled with a varying number N of $kr=2$ spherical particles. The particle refractive index is fixed at $m=1.31$. The packing density $\bar{\rho}$ varies between 1.5% ($N=100$) and 11.7% ($N=800$) for $kR=40$ and between 1.45% ($N=200$) and 4.3% ($N=600$) for $kR=50$.

ized Stokes-scattering matrix of the volume $\tilde{\mathbf{F}}(\Theta)$ [14,31,36],

$$\begin{bmatrix} I^{sca} \\ Q^{sca} \\ U^{sca} \\ V^{sca} \end{bmatrix} \propto \tilde{\mathbf{F}}(\Theta) \begin{bmatrix} I^{inc} \\ Q^{inc} \\ U^{inc} \\ V^{inc} \end{bmatrix} = \begin{bmatrix} a_1(\Theta) & b_1(\Theta) & 0 & 0 \\ b_1(\Theta) & a_2(\Theta) & 0 & 0 \\ 0 & 0 & a_3(\Theta) & b_2(\Theta) \\ 0 & 0 & -b_2(\Theta) & a_4(\Theta) \end{bmatrix} \begin{bmatrix} I^{inc} \\ Q^{inc} \\ U^{inc} \\ V^{inc} \end{bmatrix}. \tag{6}$$

This scattering matrix is a particular case of the Mueller

transformation matrix [37]. The zeros denote scattering matrix elements negligibly small (in the absolute sense) relative to the other elements at the same scattering angle. The (1,1) element $a_1(\Theta)$ is called the phase function and is normalized according to the integral condition

$$\frac{1}{2} \int_0^\pi d\Theta \sin \Theta a_1(\Theta) = 1. \tag{7}$$

The elements of the scattering matrix can be used to define specific optical observables corresponding to different types of polarization state of the incoming light. If the incident radiation is unpolarized, then the phase function characterizes the angular distribution of the scattered intensity, while the ratio $-b_1(\Theta)/a_1(\Theta)$ gives the corresponding degree of linear polarization.

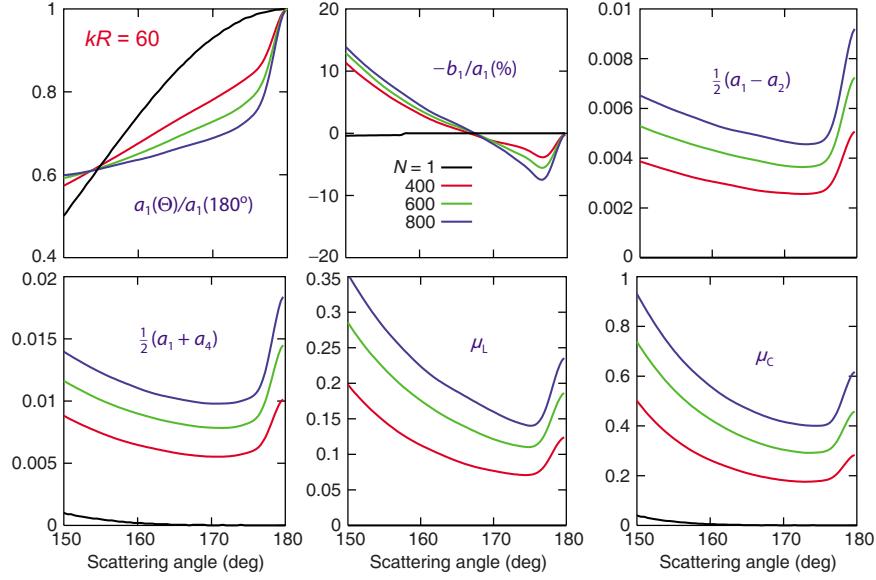


FIG. 6. (Color online) Optical characteristics of a $kR=60$ scattering volume randomly filled with a varying number N of $kr=2$ spherical particles. The particle refractive index is fixed at $m=1.31$. The packing density $\tilde{\rho}$ varies between 1.6% ($N=400$) and 3.3% ($N=800$).

If the incident radiation is polarized linearly in the scattering plane according to Eq. (2) then the angular distributions of the co-polarized and cross-polarized scattered intensities are given by

$$I_{\parallel,\parallel} = \frac{1}{2}(I^{\text{sca}} + Q^{\text{sca}}) \propto \frac{1}{2}[a_1(\Theta) + 2b_1(\Theta) + a_2(\Theta)] \quad (8)$$

and

$$I_{\perp,\parallel} = \frac{1}{2}(I^{\text{sca}} - Q^{\text{sca}}) \propto \frac{1}{2}[a_1(\Theta) - a_2(\Theta)], \quad (9)$$

respectively. The linear polarization ratio μ_L is defined as the ratio of the cross-polarized to co-polarized scattered intensities and is given by

$$\mu_L = \frac{I_{\perp,\parallel}}{I_{\parallel,\parallel}} = \frac{a_1(\Theta) - a_2(\Theta)}{a_1(\Theta) + 2b_1(\Theta) + a_2(\Theta)}. \quad (10)$$

If the incident radiation is polarized linearly in the direction normal to the scattering plane according to Eq. (4) then the angular distribution of the co-polarized scattered intensity is given by

$$I_{\perp,\perp} = \frac{1}{2}(I^{\text{sca}} + Q^{\text{sca}}) \propto \frac{1}{2}[a_1(\Theta) - 2b_1(\Theta) + a_2(\Theta)]. \quad (11)$$

If the incident radiation is polarized circularly in the counterclockwise direction when looking in the direction of propagation,

$$\mathbf{I}^{\text{inc}} = \begin{bmatrix} I^{\text{inc}} \\ 0 \\ 0 \\ V^{\text{inc}} = I^{\text{inc}} \end{bmatrix}, \quad (12)$$

then the angular distributions of the same-helicity and opposite-helicity scattered intensities are given by

$$I_{\text{sh}} = \frac{1}{2}(I^{\text{sca}} + V^{\text{sca}}) \propto \frac{1}{2}[a_1(\Theta) + a_4(\Theta)] \quad (13)$$

and

$$I_{\text{oh}} = \frac{1}{2}(I^{\text{sca}} - V^{\text{sca}}) \propto \frac{1}{2}[a_1(\Theta) - a_4(\Theta)], \quad (14)$$

respectively. The circular polarization ratio μ_C is defined as the ratio of the same-helicity to the opposite-helicity scattered intensities,

$$\mu_C = \frac{I_{\text{sh}}}{I_{\text{oh}}} = \frac{a_1(\Theta) + a_4(\Theta)}{a_1(\Theta) - a_4(\Theta)}. \quad (15)$$

The direct computer modeling of the azimuthal asymmetry and the POE is not quite straightforward since the polarization of initially unpolarized light singly scattered by a particle often has a negative branch at small phase angles [36]. This makes it problematic to reliably distinguish between the singly- and multiply-scattered negative polarization in a numerical solution of the Maxwell equations [38,39]. Therefore, for each value of m studied, we have selected a size parameter that ensures that the single-scattering polarization has a wide horizontal ‘‘shelf’’ of near-zero values at backscattering angles, thereby making any multiple-scattering polarization contribution readily identifiable and quantifiable. The resulting kr values and the corresponding single-scattering polarization curves are shown in Fig. 1(d).

The results of our extensive computations are summarized in Figs. 3–7. For reference, we also show the results computed for a single isolated spherical particle. Depending on kR , the number of constituent particles in Figs. 3–7 varies up to 900. The corresponding values of the filling factor (or particle packing density) depend on the way the latter is defined. If one defines the filling factor ρ as the ratio of the cumulative volume of the constituent particles to $3\pi R^3/4$ then ρ varies from almost zero for $N=1$ up to 34.6% for the volume with $kR=40$, $N=400$, and $kr=3.81$ ($m=1.194$).

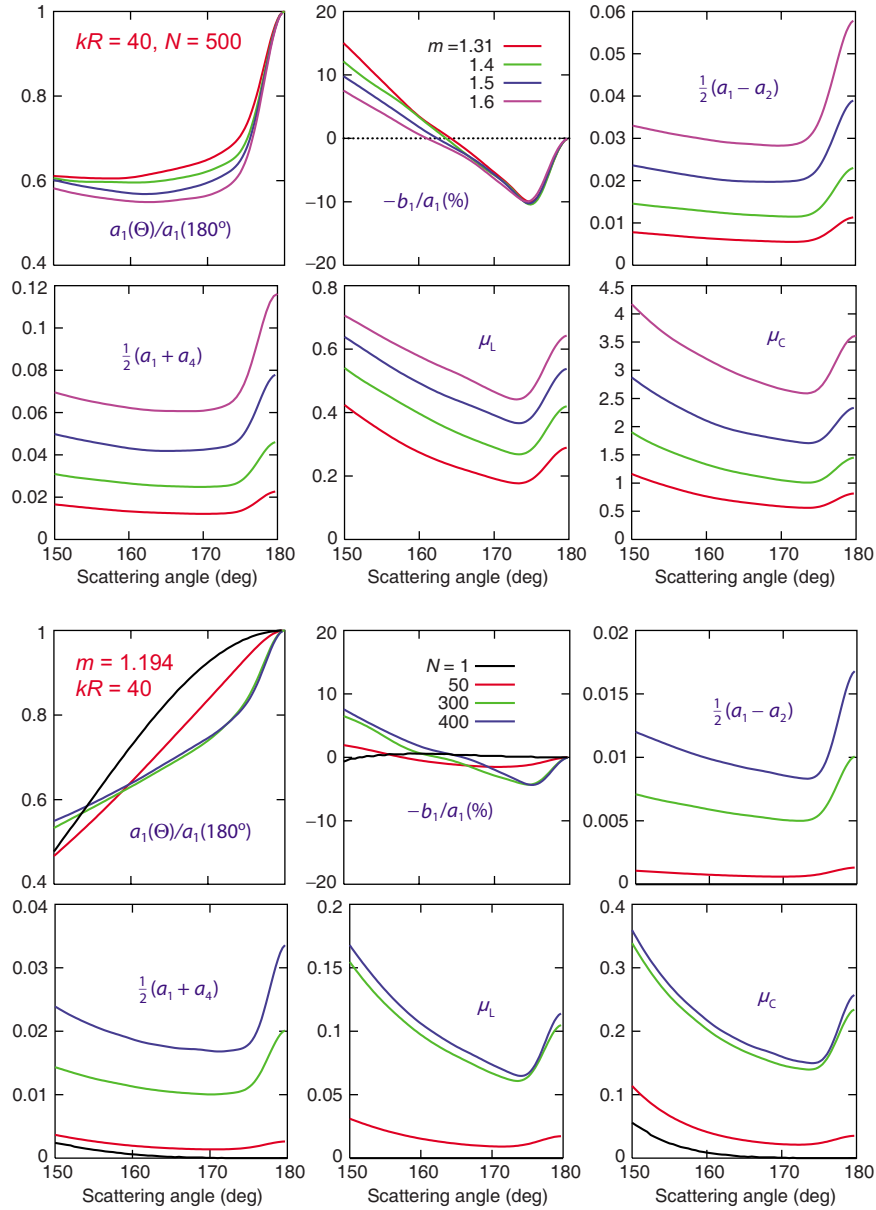


FIG. 7. (Color online) Scattering characteristics of a $kR=40$ volume randomly filled with N identical spherical particles. In the upper six diagrams, N is fixed at 500, while the particle refractive index m varies from 1.31 to 1.6. The particle refractive index in the lower six diagrams is fixed at $m=1.194$, while the number of particles N varies from 1 to 400. The packing density $\tilde{\rho}$ varies between 7.3% ($m=1.31$) and 4.1% ($m=1.6$) in the upper six diagrams and between 5.8% ($N=50$) and 46.7% ($N=400$) in the lower six diagrams.

However, this definition underestimates the actual packing density inside the volume since, by design, the constituent particles are not allowed to cross the bounding sphere with the radius R , which creates artificial empty space at the boundary of the volume [see Fig. 1(c)]. We have found that the actual packing density $\tilde{\rho}$ inside the volume defined as if the volume were infinite varies up to 46.7% for the volume with $kR=40$, $N=400$, and $kr=3.81$ ($m=1.194$); up to 41.2% for the volume with $kR=20$, $N=300$, and $kr=2$ ($m=1.31$); and up to 32.8% for the volume with $kR=30$, $N=900$, and $kr=2$ ($m=1.31$).

IV. DISCUSSION

In full agreement with the prediction of the low-density theory of CB, the numerically exact results depicted in Fig. 3

reveal a pronounced azimuthal asymmetry of the backscattering cone. Indeed, both co-polarized intensities show a strong backscattering enhancement, but the width of the $I_{\perp,\perp}$ backscattering peak is systematically smaller than that of the $I_{\parallel,\parallel}$ peak. The theoretically computed azimuthal asymmetry survives packing densities $\tilde{\rho}$ as high as 35% (and, in fact, even 46.7%), thereby implying that the azimuthal asymmetry observed for 9.6%-dense aqueous suspensions of small latex particles [8,9] was indeed caused by CB.

The co-polarized intensity peaks measured in [8,9] were significantly narrower than those in Fig. 3, which is not surprising. Indeed, the interference base for a finite scattering volume is controlled by its size parameter kR [40], whereas that for an optically thick nonabsorbing or weakly absorbing layer of discrete random medium is controlled by the product

of the wave number and the transport mean-free path [5]. The values of this product for the particulate media studied in [8,9] can be expected to be much greater than the kR values used in our computations, thereby resulting in much narrower intensity peaks.

Two expected manifestations of confined scattering geometry [40] can be clearly seen in the upper five diagrams of Fig. 3. First, the angular width of the co-polarized peaks decreases as $1/kR$, thereby testifying again to the interference origin of the peaks. Second, the peaks are rounded at $\Theta=180^\circ$, whereas those for optically thick nonabsorbing media should have a sharp triangular cusp [3,4,7] (cf. the dotted curve in Fig. 2).

As anticipated, all $-b_1(\Theta)/a_1(\Theta)$ curves for $N>1$ in Figs. 4–7 reveal the POE. Four morphological traits of the polarization minima testify to their interference multiple-scattering origin. First, the minima are absent in the single-particle curves but are present in the curves for $N>1$. Second, the phase angle of minimal polarization is independent of N , scales as $1/kR$, and is quite comparable to the angular width of the CB peak in the normalized phase function $a_1(\Theta)/a_1(180^\circ)$ (see Figs. 4–6). Third, the phase angle of minimal polarization is independent of the particle refractive index (Fig. 7). Fourthly, the polarization minima in Figs. 4–6 become increasingly asymmetric with increasing kR and start to resemble closely the polarization curve in Fig. 2 predicted by the asymptotic low-density theory of CB (note that polarization in Fig. 2 does not become positive at larger phase angles because the theoretical computation in [4] assumed a phase-angle-independent ladder component).

The effect of increasing the number of particles N in a fixed scattering volume can be expected to be twofold. On one hand, it facilitates multiple scattering and thereby should enhance the classical manifestations of CB. On the other hand, it leads to increased packing density and can eventually cause changes in the backscattering features not implied by the low-packing-density theory of CB [39]. The polarization curves clearly demonstrate both tendencies. Indeed, the depth of the POE minimum first increases as N increases from 1 to a certain kR -dependent saturation value. However, a further increase in N causes packing densities that are large enough to distort noticeably the shape of the POE minimum and decrease significantly the scattering angle of zero polarization (the so-called inversion point). The results shown in Fig. 4 suggest that the effects of packing density on the POE become significant at $\tilde{\rho}\sim 30\%$.

The results of our numerically exact computations for densely packed discrete random media indicate that the extremely narrow backscattering polarization minimum measured by Lyot eighty years ago for a particulate MgO surface [11] represents indeed the first laboratory observation of the POE caused by CB. Importantly, Lyot's polarimetric results have recently been reproduced and accompanied by intensity measurements [13]. These new laboratory results have revealed an equally narrow backscattering intensity peak, in full agreement with our numerically exact theoretical results.

Figures 4–7 also reveal other important backscattering effects implied by the asymptotic theory of CB [2], all of them becoming increasingly pronounced with growing N . In fact, the peaks in the $\frac{1}{2}(a_1-a_2)$, $\frac{1}{2}(a_1+a_4)$, μ_L , and μ_C curves are

even more indicative of their multiple-scattering origin than that in the normalized scattered intensity $a_1(\Theta)/a_1(180^\circ)$ since they are absent completely for a single spherical particle. For a fixed kR , the angular widths of all these peaks are approximately equal and are independent of the number of particles and their refractive index. Furthermore, they scale as $1/kR$, thereby confirming their CB nature. Interestingly, CB can cause either a backscattering enhancement or a backscattering “depression” in the linear polarization ratio μ_L depending on particle microphysical properties and on the optical thickness of the particulate medium (see Figs. 4–7 and [2,14,16,41,42]). These results illustrate the limited validity of the speculative belief existing in planetary remote sensing that CB can cause only a backscattering minimum in μ_L .

Our results show that the CB peaks in the $a_1(\Theta)/a_1(180^\circ)$, $\frac{1}{2}(a_1-a_2)$, $\frac{1}{2}(a_1+a_4)$, and μ_L curves are remarkably immune to the effects of packing density. However, the backscattering peak in the μ_C angular profile becomes noticeably suppressed when $\tilde{\rho}$ exceeds $\sim 30\%$ (Fig. 4), thereby revealing the same susceptibility to large filling factor values as the degree of linear polarization.

V. CONCLUDING REMARKS

The indisputable advantages of the direct computer modeling of multiple scattering by discrete random media are that it yields numerically exact results, does not involve the simplifying assumption of a small packing density, and allows one to vary all physical parameters of the scattering medium one at a time [14–16,43,44]. As a result, one is able to trace unambiguously the onset of multiple scattering as the particle number deviates from one, the evolution of various manifestations of CB with increasing N , and the eventual onset of packing density effects distorting the angular profiles of the POE and circular polarization ratio predicted by the low-density theory of CB. Based on our numerical data, we can conclude that the azimuthal asymmetry of the polarized backscattering cone and the POE observed in [8,9,11–13] for densely packed particulate media are indeed caused by CB. Another important implication is that CB is the likely cause of the uniquely narrow photometric and polarization opposition effects observed simultaneously for a class of high-albedo solar system bodies [45–51].

Our results pose an important question as to why the various manifestations of CB are so remarkably immune to packing density effects. Although the definitive answer to this question is not immediately obvious, one could speculate that even in densely packed discrete random media, the partial multiply-scattered waves [Fig. 1(a)] that involve widely separated particles still provide a significant contribution to the total scattered signal sufficient to make quite pronounced the classical multiple-scattering and CB features.

ACKNOWLEDGMENTS

We thank an anonymous reviewer for useful comments on the original manuscript. This research was supported by the NASA Radiation Sciences Program.

- [1] M. I. Mishchenko, *Astrophys. J.* **411**, 351 (1993).
- [2] M. I. Mishchenko, L. D. Travis, and A. A. Lacis, *Multiple Scattering of Light by Particles: Radiative Transfer and Coherent Backscattering* (Cambridge University Press, Cambridge, 2006).
- [3] V. D. Ozrin, *Waves Random Media* **2**, 141 (1992).
- [4] E. Amic, J. M. Luck, and Th. M. Nieuwenhuizen, *J. Phys. A* **29**, 4915 (1996).
- [5] Yu. N. Barabanenkov, Yu. A. Kravtsov, V. D. Ozrin, and A. I. Saichev, *Prog. Opt.* **29**, 65 (1991).
- [6] K. Muinonen, *Waves Random Media* **14**, 365 (2004).
- [7] E. Akkermans and G. Montambaux, *Mesosopic Physics of Electrons and Photons* (Cambridge University Press, Cambridge, 2007).
- [8] M. P. van Albada, M. B. van der Mark, and A. Lagendijk, *Phys. Rev. Lett.* **58**, 361 (1987).
- [9] M. P. van Albada, M. B. van der Mark, and A. Lagendijk, *J. Phys. D* **21**, S28 (1988).
- [10] M. I. Mishchenko, J.-M. Luck, and Th. M. Nieuwenhuizen, *J. Opt. Soc. Am. A Opt. Image Sci. Vis* **17**, 888 (2000).
- [11] B. Lyot, *Ann. Obs. Meudon* **8**, 1 (1929).
- [12] Yu. G. Shkuratov, A. A. Ovcharenko, V. A. Psarev, and S. Y. Bondarenko, *Light Scattering Rev.* **3**, 383 (2008).
- [13] Yu. Shkuratov, A. Ovcharenko, E. Zubko, O. Miloslavskaya, K. Muinonen, J. Piironen, R. Nelson, W. Smythe, V. Rosenbush, and P. Helfenstein, *Icarus* **159**, 396 (2002).
- [14] M. I. Mishchenko, L. Liu, D. W. Mackowski, B. Cairns, and G. Videen, *Opt. Express* **15**, 2822 (2007).
- [15] M. I. Mishchenko, *Rev. Geophys.* **46**, RG2003 (2008).
- [16] M. I. Mishchenko and L. Liu, *Appl. Opt.* **48**, 2421 (2009).
- [17] L. Tsang, J. A. Kong, and R. T. Shin, *Theory of Microwave Remote Sensing* (Wiley, New York, 1985).
- [18] V. A. Babenko, L. G. Astafyeva, and V. N. Kuzmin, *Electromagnetic Scattering in Disperse Media* (Praxis, Chichester, UK, 2003).
- [19] M. I. Mishchenko, *J. Quant. Spectrosc. Radiat. Transf.* **110**, 1210 (2009).
- [20] M. I. Mishchenko, *Appl. Opt.* **41**, 7114 (2002).
- [21] Yu. N. Gnedin and A. Z. Dolginov, *Sov. Phys. JETP* **18**, 784 (1964).
- [22] Yu. N. Barabanenkov, *Radiophys. Quantum Electron.* **16**, 65 (1973).
- [23] K. M. Watson, *J. Math. Phys.* **10**, 688 (1969).
- [24] Yu. N. Barabanenkov, *Sov. Phys. Usp.* **18**, 673 (1975).
- [25] Y. Kuga and A. Ishimaru, *J. Opt. Soc. Am. A* **1**, 831 (1984).
- [26] L. Tsang and A. Ishimaru, *J. Opt. Soc. Am. A* **1**, 836 (1984).
- [27] M. P. Van Albada and A. Lagendijk, *Phys. Rev. Lett.* **55**, 2692 (1985).
- [28] P.-E. Wolf and G. Maret, *Phys. Rev. Lett.* **55**, 2696 (1985).
- [29] M. P. van Albada and A. Lagendijk, *Phys. Rev. B* **36**, 2353 (1987).
- [30] T. Iwai, H. Furukawa, and T. Asakura, *Opt. Rev.* **2**, 413 (1995).
- [31] J. W. Hovenier, C. van der Mee, and H. Domke, *Transfer of Polarized Light in Planetary Atmospheres* (Kluwer, Dordrecht, The Netherlands, 2004).
- [32] Yu. G. Shkuratov, K. Muinonen, E. Bowell, K. Lumme, J. I. Peltoniemi, M. A. Kreslavsky, D. G. Stankevich, V. P. Tishkovets, N. V. Opanasenko, and L. Y. Melkumova, *Earth, Moon, and Planets* **65**, 201 (1994).
- [33] D. W. Mackowski, *J. Quant. Spectrosc. Radiat. Transf.* **100**, 237 (2006).
- [34] D. W. Mackowski and M. I. Mishchenko, *J. Opt. Soc. Am. A Opt. Image Sci. Vis* **13**, 2266 (1996).
- [35] D. W. Mackowski, *J. Opt. Soc. Am. A Opt. Image Sci. Vis* **11**, 2851 (1994).
- [36] M. I. Mishchenko, L. D. Travis, and A. A. Lacis, *Scattering, Absorption, and Emission of Light by Small Particles* (Cambridge University Press, Cambridge, 2002). <http://www.giss.nasa.gov/~crmim/books.html>.
- [37] Ch. Brosseau, *Fundamentals of Polarized Light: A Statistical Optics Approach* (Wiley, New York, 1998).
- [38] E. V. Petrova, V. P. Tishkovets, and K. Jockers, *Icarus* **188**, 233 (2007).
- [39] V. P. Tishkovets, *J. Quant. Spectrosc. Radiat. Transf.* **109**, 2665 (2008).
- [40] S. Etemad, R. Thompson, M. J. Andrejco, S. John, and F. C. MacKintosh, *Phys. Rev. Lett.* **59**, 1420 (1987).
- [41] J. M. Dlugach and M. I. Mishchenko, *J. Quant. Spectrosc. Radiat. Transf.* **106**, 21 (2007).
- [42] M. I. Mishchenko and J. M. Dlugach, *J. Quant. Spectrosc. Radiat. Transf.* **110**, 1706 (2009).
- [43] S. Tseng, *Opt. Commun.* **281**, 1986 (2008).
- [44] Y. Okada and A. A. Kokhanovsky, *J. Quant. Spectrosc. Radiat. Transf.* **110**, 902 (2009).
- [45] V. K. Rosenbush, V. A. Avramchuk, A. E. Rosenbush, and M. I. Mishchenko, *Astrophys. J.* **487**, 402 (1997).
- [46] V. K. Rosenbush and N. N. Kiselev, *Icarus* **179**, 490 (2005).
- [47] V. K. Rosenbush, N. N. Kiselev, V. G. Shevchenko, K. Jockers, N. M. Shakhovskoy, and Yu. S. Efimov, *Icarus* **178**, 222 (2005).
- [48] M. I. Mishchenko, V. K. Rosenbush, and N. N. Kiselev, *Appl. Opt.* **45**, 4459 (2006).
- [49] V. Rosenbush, N. Kiselev, and V. Avramchuk, *J. Quant. Spectrosc. Radiat. Transf.* **100**, 325 (2006).
- [50] V. Rosenbush, V. Shevchenko, N. Kiselev, A. Sergeev, N. Shakhovskoy, F. Velichko, S. Kolesnikov, and N. Karpov, *Icarus* **201**, 655 (2009).
- [51] N. Kiselev, V. Rosenbush, F. Velichko, and S. Zaitsev, *J. Quant. Spectrosc. Radiat. Transf.* **110**, 1713 (2009).